Chinese Chemical Letters 34 (2023) 107844

Contents lists available at ScienceDirect

Chinese Chemical Letters

journal homepage: www.elsevier.com/locate/cclet

Lower oxygen vacancy concentration in $BiPO_4$ with unexpected higher photocatalytic activity

Jun Xiong [a,*], Haoxue Huang [a], Bo Lin [c], Jiexiang Xia [a], Jun Di [b,*]

[a] School of Chemistry and Chemical Engineering, Institute for Energy Research, Jiangsu University, Zhenjiang 212013, China
[b] School of Chemistry and Chemical Engineering, National Special Superfine Powder Engineering Research Center, Nanjing University of Science and Technology, Nanjing 210094, China
[c] School of Chemical Engineering and Technology, Xi'an Jiaotong University, Xi'an 710049, China

ARTICLE INFO

Article history:
Received 29 June 2022
Revised 5 September 2022
Accepted 21 September 2022
Available online 24 September 2022

Keywords:
$BiPO_4$
Photocatalytic
Oxygen vacancy
Ciprofloxacin
Energy band structure

ABSTRACT

Defect engineering has been demonstrated to be an appealing strategy to boost the photocatalytic activity of materials. However, can higher defect concentration bring about higher photocatalytic activity? This is an open question. In this work, $BiPO_4$ photocatalysts with controllable oxygen vacancy concentrations were successfully synthesized. The photocatalytic activity of the obtained $BiPO_4$ photocatalysts was determined by the removal of ciprofloxacin and 4-chlorophenol, as well as CO_2 photoreduction. The $BiPO_4$ materials with lower oxygen vacancy concentration could display unexpected higher photocatalytic efficiency. Through the investigation of different factors which may affect the photocatalytic performance, such as crystal structure, morphology, specific surface area, defect, and energy band structure, it can be found that the energy band structure difference was responsible for the enhanced photocatalytic activity.

With the rapid development of economy, the environmental pollution issue has become increasingly prominent. For example, the phenols chemicals such as 4-chlorophenol has been massive discharged due to the industrial by-product or by chlorination, which was potentially carcinogenic and mutagenic to human [1]. The plentiful employment of antibiotics result in the excess emission as active form pharmaceutically, which aggravate biological drug resistance and affect the ecosystem. Moreover, these phenols chemicals and antibiotics were stubborn and difficult to entirely remove through the conventional treatment methods. Semiconductor photocatalysis has attracted massive attention towards environmental purification [2]. The critical point to acquire high-activity lie on the strong oxidation ability of semiconductor under light excitation. Although the semiconductor materials such as g-C_3N_4, $W_{18}O_{49}$, BiOX, have been widely developed [3–7], the efficiency was limited owning to the high potential of valence band (VB) which cannot endow the powerful oxidizing ability.

As one of the oxyacid salt photocatalysts, $BiPO_4$ displayed numerous advantages including photoelectric properties, low cost, nontoxicity, and outstanding photocatalytic efficiency [8,9]. Due to the deeper VB position, $BiPO_4$ can display more attractive activity than many photocatalysts towards pollutant removal. To optimize the photocatalytic behavior of $BiPO_4$ materials, many strategies have been employed such as heteroatom doping [10,11], defect adjusting [12–14], phase junction [15], surface modification [16–18] and semiconductors coupling [19–23]. Although the photocatalytic activity of the obtained $BiPO_4$ materials can be moderate increased, it was still of great importance and urgency to explore suitable strategy to further improve the photocatalytic performance for practical applications.

Previous studies demonstrated that engineering defects into materials can effectively improve the photocatalytic activity [24–30]. For example, Li's group found that the formation of "Bi-O" dimer vacancy pairs could result in the reduction in band gap and reduce the recombination rate of photogenerated charge carriers, which were responsible for the improved photocatalytic performance for pollutant removal [24]. Xiong's group found that the construction of oxygen defects on WO_3 nanosheets was beneficial to oxygen chemisorption and thus facilitate the formation of superoxide radicals [25]. As a result, the photocatalytic organic synthesis of amines to corresponding imines can be greatly promoted. Therefore, defects engineering seems to be a desirable method to tune the photocatalytic performance of $BiPO_4$. However, the defects can not only serve as separation center for photogenerated charge to boost the photocatalytic performance but also can work as recombination center to decrease the photocatalytic activity. It needs fur-

* Corresponding authors.
E-mail addresses: xiongjun@ujs.edu.cn (J. Xiong), lydijun@163.com (J. Di).

https://doi.org/10.1016/j.cclet.2022.107844
1001-8417/

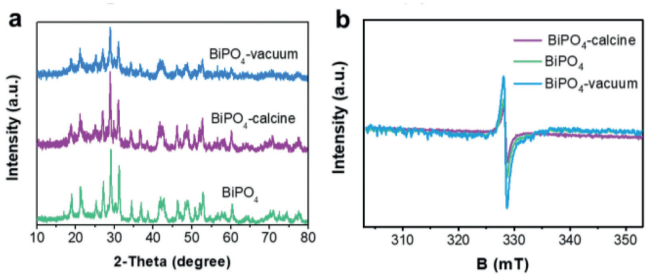

Fig. 1. (a) XRD patterns and (b) EPR spectra of the as-synthesized $BiPO_4$, $BiPO_4$-calcine, and $BiPO_4$-vacuum materials.

ther study whether the higher defect concentration can inevitably bring about higher activity.

In this system, $BiPO_4$ materials with different oxygen vacancy concentration have been controlled prepared to study the affection of oxygen vacancy towards photocatalytic behavior of $BiPO_4$. It is worth noting that $BiPO_4$ materials with lower oxygen vacancy concentration can show higher photocatalytic activity for pollutant removal. The mechanism for the improved photocatalytic performance of $BiPO_4$ was also investigated.

X-ray diffraction (XRD) analysis was employed to study the crystallinity and phase structure of the as-synthesized samples and the result was shown in Fig. 1a. The diffraction peaks of the as-synthesized sample match well with monoclinic $BiPO_4$ (JCPDS card No. 15-0767), with the peaks located at $2\theta = 11.9°$, 21.4°, 25.4°, 27.1°, 29.1°, 31.3°, 34.5°, 37.0°, 41.9°, 42.8°, 46.4° and 52.8° can be indexed to the (011), ($\bar{1}$11), (111), (200), (120), (012), ($\bar{2}$02), (112), ($\bar{1}$30), ($\bar{1}$31), (212) and (040) crystal planes. After further vacuum activation or annealing, no distinct variation can be observed relative to that of $BiPO_4$, revealing the further treatment did not destroy crystal structure. The detailed structural information of the prepared $BiPO_4$, $BiPO_4$-vacuum, $BiPO_4$-calcine materials were further determined by Fourier transform infrared (FT-IR). It can be seen from Fig. S1 (Supporting information) that absorption peaks centered at 524 and 554 cm^{-1} were attributed to the $\upsilon 4$ vibrational behavior of PO_4^{3-} ions, while the peaks of $\upsilon 3$ stretching modes can be seen from 900 to 1100 cm^{-1} [31]. The similar FT-IR profiles of $BiPO_4$, $BiPO_4$-vacuum, $BiPO_4$-calcine materials suggested the successful preparation of $BiPO_4$ and main structure was well maintained.

To determine the oxygen vacancy in the prepared different $BiPO_4$ samples, low-temperature electron paramagnetic resonance (EPR) analysis was carried out. As shown in Fig. 1b, the typical signal at $g = 2.001$ can be found for these three materials which powerful certify the existence of oxygen vacancies [32]. The 1,3-butanediol could easily react with the oxygen in the $BiPO_4$ to produce oxygen vacancies during the synthetic process, and the similar result can also be found in other systems [33]. It is noted that the $BiPO_4$ displayed higher intensity than $BiPO_4$-calcine sample and the $BiPO_4$-vacuum materials exhibited the highest signal. This result indicated that the vacuum activation process can further create oxygen vacancies on $BiPO_4$, while annealing at atmosphere may repair the oxygen vacancies.

X-ray photoelectron spectroscopy (XPS) was employed to determine the surface composition of the obtained samples. The survey spectrum (Fig. 2a) of the obtained $BiPO_4$ samples were consist of Bi, P, O and C elements, in which the existence of C was ascribed to adventitious carbon species from the XPS instrument. From high-resolution Bi 4f spectra (Fig. 2b), the peaks centered at 159.7 and 164.9 eV corresponded to the Bi $4f_{7/2}$ and Bi $4f_{5/2}$ of Bi^{3+} in $BiPO_4$ materials. In high-resolution O 1s spectra (Fig. 2c), the peak located at 530.9 eV was assigned to Bi-O bonds, and the peak at 532.4 eV was derived from O-atoms in the vicinity of an O vacancy [34]. The area corresponded to O vacancy showed difference among these three materials. The $BiPO_4$-vacuum sample showed the largest area and $BiPO_4$ was larger than that of $BiPO_4$-calcine, indicating the oxygen vacancy can be further increased by vacuum activation and annealing decrease the oxygen vacancy. The binding energy at 133.1 eV can be assigned to P 2p peak in $BiPO_4$ materials (Fig. 2d). The above results suggested the $BiPO_4$ materials with different oxygen vacancy concentration have been controlled prepared.

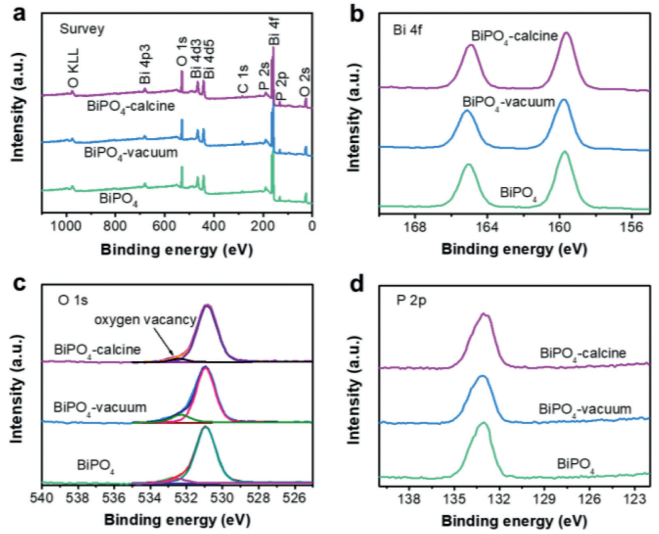

Fig. 2. XPS spectra of $BiPO_4$, $BiPO_4$-calcine, and $BiPO_4$-vacuum samples. (a) Survey of the samples; (b) Bi 4f; (c) O 1s and (d) P 2p.

To study the affection of oxygen vacancy on the light absorption ability, the UV-vis diffuse reflectance spectra (DRS) was carried out on the $BiPO_4$, $BiPO_4$-vacuum and $BiPO_4$-calcine samples. As shown in Fig. S2a (Supporting information), $BiPO_4$ materials with different oxygen vacancy concentrations displayed obvious difference of the light absorption region. The $BiPO_4$-calcine materials with the lowest oxygen vacancy concentration showed the photoabsorption of 200–300 nm, indicating the $BiPO_4$ was intrinsic UV-light response photocatalyst. With the increase of oxygen vacancy concentration, the light absorption region extended to visible and infrared region, and this phenomenon was similar to that in literatures [25,28]. The band gap energies of these $BiPO_4$ samples can be thus calculated by the Kubelka-Munk function. As shown in Fig. S2b (Supporting information) the band gap of $BiPO_4$-calcine, $BiPO_4$, and $BiPO_4$-vacuum materials can be estimated to be 4.26, 3.89 and 3.66 eV, respectively.

The morphology and microstructure of the prepared $BiPO_4$ materials with different oxygen vacancy concentrations were observed by transmission electron microscopy (TEM) images. From Figs. 3a and b, it can be seen that the $BiPO_4$ sample showed the nanoparticle morphology with the average size about 40 nm. After further annealing (Figs. 3c and d) to decrease the oxygen vacancy or vacuum activation (Figs. 3e and f) to increase the oxygen vacancy concentration, the morphology did not show distinct variation. This result demonstrated that the morphology difference may be not the main factor to affect the photocatalytic performance in this system.

As is well known, the specific surface area of photocatalysts have important influence on the photocatalytic performance due to the larger specific surface area could adsorb more pollutant and active species to form a partial high concentration [35]. The BET specific surface area of $BiPO_4$, $BiPO_4$-calcine and $BiPO_4$-vacuum materials were investigated by nitrogen adsorption-desorption isotherms. As shown in Figs. S3–S5 (Supporting information),

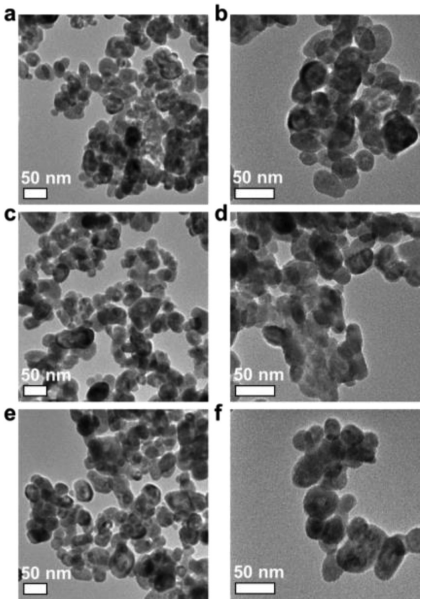

Fig. 3. TEM images of the (a, b) $BiPO_4$, (c, d) $BiPO_4$-calcine and (e, f) $BiPO_4$-vacuum samples.

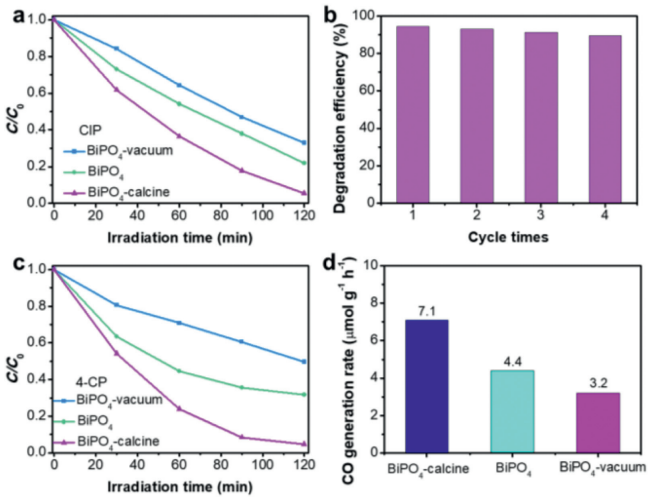

Fig. 4. (a) Photocatalytic degradation of CIP in the presence of $BiPO_4$, $BiPO_4$-vacuum and $BiPO_4$-calcine materials under UV light irradiation. (b) Cycle performance of $BiPO_4$-calcine material for CIP degradation. (c) Photocatalytic degradation of 4-CP over $BiPO_4$, $BiPO_4$-vacuum and $BiPO_4$-calcine. (d) Photocatalytic CO_2 reduction to yield CO over $BiPO_4$, $BiPO_4$-vacuum and $BiPO_4$-calcine.

all the samples displayed the type IV isotherms with a H3 hysteresis loop. The BET surface areas of $BiPO_4$, $BiPO_4$-calcine and $BiPO_4$-vacuum samples were measured to be 28.8, 21.8 and 23.7 m^2/g, respectively. The annealing and vacuum activation treatment did not have significant influence on the BET surface areas and it can be assumed that the specific surface area may be not the main activity-determining factor in this system.

It has been reported that the formed oxygen vacancies could serve as separation centers to promote the separation of photogenerated electrons and holes [12,32]. In this system, the steady photoluminescence (PL) spectroscopy was employed to study the charge separation efficiency of the obtained $BiPO_4$ materials. As shown in Fig. S6a (Supporting information), the $BiPO_4$-vacuum samples displayed decreased PL intensity than that of $BiPO_4$-calcine samples, suggesting the lower recombination rate of charge carriers in $BiPO_4$-vacuum samples [36]. Since the high oxygen vacancy concentration in $BiPO_4$-vacuum materials, the oxygen vacancies could effectively facilitate the separation of charge carriers and thus ensure the decreased PL intensity. To further insight the charge transfer and recombination processes in the $BiPO_4$ materials, electrochemical impedance spectroscopy (EIS) was carried out and the result was shown in Fig. S6b (Supporting information). The Nyquist arc radius in the EIS analysis revealed the solid state interface layered resistance and the surface charges transfer resistance [37]. The arc radius of $BiPO_4$-vacuum was smaller than that of $BiPO_4$-calcine sample, meaning the $BiPO_4$-vacuum possess smaller resistance than that of $BiPO_4$-calcine and thus could achieve the higher charge separation efficiency.

The photocatalytic performance of the obtained $BiPO_4$ materials with different oxygen vacancy concentrations was evaluated by the degradation of colourless antibiotic agent ciprofloxacin (CIP). Massive emission of CIP into aquatic environments will aggravate antibiotic resistance and affect the ecological environment. It is highly desirable to found effective method to remove the CIP from aquatic environments. As shown in Fig. 4a, 78% of CIP can be removed by $BiPO_4$ sample under UV light irradiation for 120 min, indicating the CIP can be degraded by $BiPO_4$ materials. However, when the oxygen vacancies were further created in $BiPO_4$ by vacuum activation, the photocatalytic performance decreased for the removal of CIP. Only 67% of CIP can be degraded by $BiPO_4$-vacuum sample within the same time under UV light irradiation. Through annealing to further decrease the oxygen vacancy concentration, the photocatalytic degradation efficiency can be improved to 94.4% for CIP within 120 min. The result of total organic carbon experiment shows 63% of CIP can be mineralized after 4 h irradiation over $BiPO_4$-calcine, revealing the CIP can be effective degraded by $BiPO_4$-calcine materials. The result of photocatalytic degradation of CIP suggested that the lower oxygen vacancy concentration in $BiPO_4$ could bring about higher photocatalytic activity, which was inconsistent with the results in previous reports. Moreover, no obvious activity loss can be found after 4 times cycles, suggesting good stability of $BiPO_4$-calcine for photodegradation (Fig. 4b). To further prove the activity law, the photocatalytic behavior of the obtained materials was evaluated by the removal of 4-chlorophenol (4-CP). As shown in Fig. 4c, 50.4%, 68.3% and 95.3% of 4-CP can be removed by $BiPO_4$-vacuum, $BiPO_4$ and $BiPO_4$-calcine samples, respectively. The $BiPO_4$-calcine materials with the lowest oxygen vacancy concentration also displayed the optimal photocatalytic activity. In addition to photodegradation, the performance of the prepared samples was evaluated by CO_2 photoreduction (Fig. 4d). The $BiPO_4$-calcine showed higher photoreduction activity to yield CO, with the generation rate arrive 7.1 μmol g^{-1} h^{-1}, higher than that of $BiPO_4$ (4.4 μmol g^{-1} h^{-1}) and $BiPO_4$-vacuum (3.2 μmol g^{-1} h^{-1}). Since the $BiPO_4$-vacuum, $BiPO_4$ and $BiPO_4$-calcine samples have similar morphology and specific surface area, the morphology and specific surface area difference may be not the main factor to determine the ultimate photocatalytic performance. Moreover, the $BiPO_4$-vacuum displayed higher charge separation efficiency than $BiPO_4$-calcine, which was also do not agree with the photocatalytic result.

To gain further insight into the intrinsic reason of the materials with lower oxygen vacancy concentration exhibit the higher photocatalytic activity, the XPS valence spectra was performed. It can be seen from Fig. 5a that the $BiPO_4$-vacuum, $BiPO_4$ and $BiPO_4$-calcine samples displayed the maximum energy edge of the VB at about 2.69, 2.56 and 2.44 eV, respectively. According to the band gap obtained from DRS analysis and the formula $E_{CB} = E_{VB} - E_g$, the conduction band (CB) edge of $BiPO_4$-vacuum, $BiPO_4$ and $BiPO_4$-calcine samples can be estimated to be −0.97, −1.34 and −1.82 eV, respectively. The $BiPO_4$-calcine materials showed the up-shifted CB and VB edges when compared with $BiPO_4$ and $BiPO_4$-vacuum

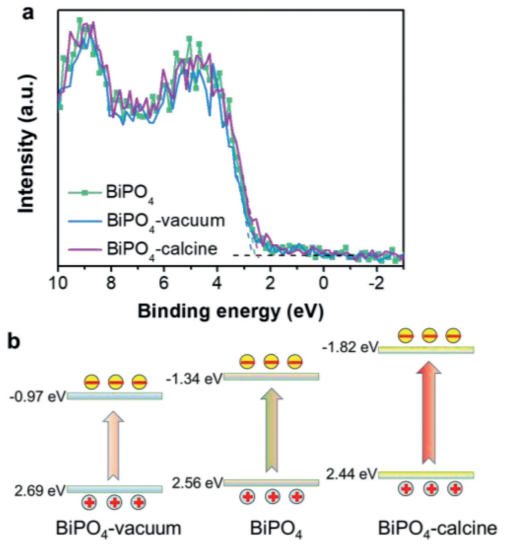

Fig. 5. (a) XPS valence-band spectra and (b) schematic of energy band structure of the $BiPO_4$, $BiPO_4$-vacuum and $BiPO_4$-calcine materials.

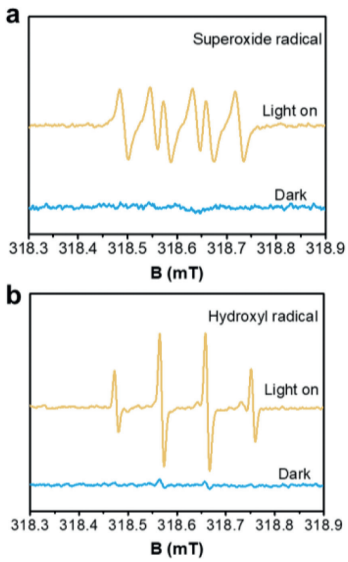

Fig. 6. DMPO spin-trapping ESR spectra recorded with $BiPO_4$-calcine materials in (a) methanol dispersion and (b) aqueous dispersion under UV light irradiation.

(Fig. 5b). The more negative CB position favors the CO_2 reduction to yield CO. The upshifting of the CB edge could generate more reductive photogenerated electrons to react with molecular oxygen to yield $O_2^{\bullet-}$. The $O_2^{\bullet-}$ was one of the important active species which can effectively degrade the pollutants. In addition, the $BiPO_4$-calcine showed the improved VB width relative to $BiPO_4$ and $BiPO_4$-vacuum. The VB width could intrinsically dominate the mobility of the photogenerated holes. The wider VB width could bring about faster mobility of holes and thus the better photooxidation efficacy can be achieved [38,39]. As a result, the $BiPO_4$-calcine could display the increased photocatalytic activity.

To further determine the active species produced during the photodegradation process, the ESR spin-trap technique was performed. The 5,5-dimethyl-1-pyrroline N-oxide (DMPO) was used as radicals trapping agent to generate the stable DMPO-$O_2^{\bullet-}$ or DMPO-$^{\bullet}$OH in methanol and water, respectively. As shown in Fig. 6a, the signal of DMPO-$O_2^{\bullet-}$ can be observed over $BiPO_4$-calcine materials under UV light irradiation which indicated the $O_2^{\bullet-}$ can be generated over $BiPO_4$. Considering the $E^0(O_2/O_2^{\bullet-})$ was about −0.33 eV, the electrons on the CB were negative enough to activate the oxygen *via* single electron transfer. At the same time, the four-fold peaks with the intensity ratio 1:2:2:1 can be seen, which was attributed to the DMPO-$^{\bullet}$OH signal (Fig. 6b). The $E^0(^{\bullet}OH/OH^-)$ was 2.38 eV *vs.* NHE, thus the holes on the VB of $BiPO_4$-calcine could oxidize OH^- to yield $^{\bullet}$OH. Therefore, the excellent photocatalytic activity of $BiPO_4$-calcine (with the lowest oxygen vacancy concentration) was derived from the synergistic effect of $O_2^{\bullet-}$, $^{\bullet}$OH and holes. Taking the above-mentioned factors into consideration, the energy band structure variation may be the main factor dominating the photocatalytic performance in this system.

In summary, $BiPO_4$ materials with different oxygen vacancy concentrations have been controlled prepared through 1,3-butanediol assisted solvothermal method, vacuum chemical activation and annealing processes. The $BiPO_4$-calcine with the lowest oxygen vacancy concentration displayed the optimal photocatalytic performance for the degradation of CIP and 4-CP and CO_2 photoreduction to yield CO. According to different characterizations, the enhanced photocatalytic activity can be ascribed to the varied energy band structure with both the upshifting of CB and VB positions. This study can be extended to prepare other photocatalysts with controllable oxygen vacancy concentration and may provide some insight of the mechanism.

Declaration of competing interest

The authors declare that they have no known competing financial interests or personal relationships that could have appeared to influence the work reported in this paper.

Acknowledgments

This work was financially supported by the National Natural Science Foundation of China (No. 22002014), the Funding for scientific research startup of Jiangsu University (No. 20JDG15), Fundamental Research Funds for the Central Universities (No. 30922010302) and Start-Up Grant (No. AE89991/397) from Nanjing University of Science and Technology.

Supplementary materials

Supplementary material associated with this article can be found, in the online version, at doi:10.1016/j.cclet.2022.107844.

References

[1] J.X. Yuan, Q. Wu, P. Zhang, et al., Environ. Sci. Technol. 46 (2012) 2330–2336.
[2] Z.W. Jiang, Y.C. Zou, T.T. Zhao, et al., Angew. Chem. Int. Ed. 59 (2020) 3300–3306.
[3] J.H. Zou, W.H. Zhou, L.Q. Huang, et al., J. Catal. 400 (2021) 347–354.
[4] G.M. Liu, H.Q. Lv, Y.B. Zeng, et al., Trans. Tianjin Univ. 27 (2021) 139–146.
[5] J. Di, J.X. Xia, M.X. Ji, et al., Appl. Catal. B: Environ. 183 (2016) 254–262.
[6] J. Di, J.X. Xia, M.X. Ji, et al., Nanoscale 7 (2015) 11433–11443.
[7] J. Li, L. Zhang, J.W. Li, et al., ACS Sustain. Chem. Eng. 7 (2019) 14023–14030.
[8] R. Kumar, P. Raizada, A.A.P. Khan, et al., J. Mater. Sci. Technol. 108 (2022) 208–225.
[9] J. Xu, L. Li, C.S. Guo, Y. Zhang, W. Meng, Appl. Catal. B: Environ. 130-131 (2013) 285–292.
[10] Y.F. Liu, Y.H. Lv, Y.Y. Zhu, et al., Appl. Catal. B: Environ. 147 (2014) 851–857.
[11] J. Di, J. Chen, M.X. Ji, et al., Chem. Eng. J. 313 (2017) 1477–1485.
[12] A.N. El-Shazly, M.A. Hamza, N.K. Allam, Int. J. Hydrog. Energy 46 (2021) 23214–23224.
[13] Y.Y. Zhu, Q. Ling, Y.F. Liu, H. Wang, Y.F. Zhu, Appl. Catal. B: Environ. 187 (2016) 204–211.
[14] Z. Wei, Y.F. Liu, J. Wang, et al., Nanoscale 7 (2015) 13943–13950.
[15] Y.Y. Zhu, Y.F. Liu, Y.H. Lv, et al., J. Mater. Chem. A 2 (2014) 13041–13048.
[16] J. Di, J.X. Xia, X.L. Chen, et al., Carbon 114 (2017) 601–607.
[17] W.J. Yang, S.H. Tang, Z. Wei, et al., Chem. Eng. J. 421 (2021) 129720.
[18] F. Tian, H.P. Zhao, G.F. Li, et al., ChemSusChem 9 (2016) 1579–1585.
[19] Y.Y. Zhu, Y.J. Wang, Q. Ling, Y.F. Zhu, Appl. Catal. B: Environ. 200 (2017) 222–229.
[20] S. Obregón, Y.F. Zhang, G. Colón, Appl. Catal. B: Environ. 184 (2016) 96–103.

[21] S. Ganguli, C. Hazra, M. Chatti, T. Samanta, V. Mahalingam, Langmuir 32 (2016) 247–253.
[22] J. Mei, Y. Tao, C. Gao, et al., Appl. Catal. B: Environ. 285 (2021) 119841.
[23] N. Liu, N. Lu, H.T. Yu, S. Chen, X. Quan, Chem. Eng. J. 428 (2022) 132116.
[24] G. Zhang, Z.Y. Hu, M. Sun, et al., Adv. Funct. Mater. 25 (2015) 3726–3734.
[25] N. Zhang, X.Y. Li, H.C. Ye, et al., J. Am. Chem. Soc. 138 (2016) 8928–8935.
[26] S.Q. Wu, J.B. Wang, Q.C. Li, et al., Trans. Tianjin Univ. 27 (2021) 155–164.
[27] Z. Shen, Y.P. Zhou, Y. Guo, et al., Chin. Chem. Lett. 32 (2021) 2524–2528.
[28] J. Di, C. Chen, C. Zhu, et al., Adv. Energy Mater. 11 (2021) 2102389.
[29] Z.M. Xu, J.Z. Cao, X. Chen, L.Y. Shi, Z.F. Bian, Trans. Tianjin Univ. 27 (2021) 147–154.
[30] X.A. Dong, Z.H. Cui, X. Shi, et al., Angew. Chem. Int. Ed. 61 (2022) e202200937.
[31] C.S. Pan, J. Xu, Y. Chen, Y.F. Zhu, Appl. Catal. B: Environ. 115-116 (2012) 314–319.
[32] X.L. Zu, Y. Zhao, X.D. Li, et al., Angew. Chem. Int. Ed. 60 (2021) 13840–13846.
[33] H. Li, J. Shang, Z.H. Ai, L.Z. Zhang, J. Am. Chem. Soc. 137 (2015) 6393–6399.
[34] Y.X. Zhao, L.R. Zheng, R. Shi, et al., Adv. Energy Mater. 10 (2020) 2002199.
[35] C.X. Zheng, G.P. He, X. Xiao, et al., Appl. Catal. B: Environ. 205 (2017) 201–210.
[36] B. Lin, B.W. Ma, J.G. Chen, et al., Chin. Chem. Lett. 33 (2022) 943–947.
[37] P. Yan, Q. Ren, F.Y. Zhong, et al., Chin. Chem. Lett. 33 (2022) 3161–3166.
[38] G. Liu, P. Niu, C.H. Sun, et al., J. Am. Chem. Soc. 132 (2010) 11642–11648.
[39] J. Di, J.X. Xia, M.X. Ji, et al., J. Mater. Chem. A 3 (2015) 15108–15118.